Geosci. Model Dev. Discuss., 4, 2893–2936, 2011
www.geosci-model-dev-discuss.net/4/2893/2011/
doi:10.5194/gmdd-4-2893-2011

Geoscientific Model Development Discussions

Importance of the surface size distribution of erodible material: an improvement of the Dust Entrainment And Deposition DEAD

M. Mokhtari[1,2], **L. Gomes**[1], **P. Tulet**[1,3], **and T. Rezoug**[4]

[1]METEO-France, URA1357, CNRM/GAME, 42 av G. Coriolis, 31057 Toulouse, France
[2]Office National de la Météorologie (ONM), Algeria
[3]LACY, Université de La Réunion, 15 avenue René Cassin, 97715 Saint-Denis, France
[4]Laboratoire des Sciences Aéronautiques (Blida), Algeria

Received: 20 September 2011 – Accepted: 12 October 2011 – Published: 10 November 2011

Correspondence to: M. Mokhtari (m_morad06@yahoo.fr)

Published by Copernicus Publications on behalf of the European Geosciences Union.

Abstract

This paper is based on dust aerosol cycle modelling in the atmospheric model ALADIN (Aire Limitée Adaptation dynamique Développement InterNational) coupled with the EXternalised SURFace scheme SURFEX. Its main goal is to create a global mineral dust emission parameterization compatible with the global database of land surface parameters ECOCLIMAP and the Food and Agriculture Organization (FAO) soil type database in SURFEX, based on both Shao (1993) and Marticorena and Bergametti (1995) parameterizations. An arrangement on the Dust Entrainment And Deposition scheme (DEAD) is proposed in this paper by introducing the geographic variation of surface size distribution, the Marticorena and Bergametti (1995) formulation of horizontal saltation flux and the Shao (2001) formulation of sandblasting efficiency α. To show the importance of the modifications introduced in the code DEAD, both sensitivity and comparative studies are realized in 0 dimensions (0-D) and then in 3 dimensions (3-D) between the old DEAD and that developed in this paper. The results in the 0-D simulations indicate that the developed DEAD scheme represents the dust source emission better, particularly in the Bodélé depression and provides a reasonable friction threshold velocity. In 3-D simulations, small differences are found between the DEAD and developed DEAD schemes for the simulated Aerosol Optical Depth (AOD) compared with the photometer AErosol RObotic NETwork (AERONET) measurements available in the African Monsoon Multidisciplinary Analyses (AMMA) databases. But, for the surface concentration a remarkable improvement is noted for the developed DEAD scheme.

1 Introduction

Substantial impacts of mineral dust aerosols on climate and environment have increased recently, creating a need to better understand and eventually predict the atmospheric dust cycle, which is involved in direct radiative forcing processes (Tegen et al.,

GMDD

4, 2893–2936, 2011

1996), nutrient transport (Martin, 1990; Swap et al., 1992), land-use change (Nicholson et al., 2000) and ecosystem health (Prospero, 1999; Shinn et al., 2000). Along these lines, several numerical dust models have been developed (Tegen and Fung, 1994; Nickovic and Dobricic, 1996; Nickovic et al., 2001) and used for studying dust processes. The first difficulty in evaluating the impacts of dust aerosols on climate and environment is to correctly determine their atmospheric concentration. To do so, it is necessary to rigorously represent their emissions in order to predict their distribution in time and space and their intensity/frequency.

The mineral dust emissions from arid and semi-arid areas are strongly influenced by surface characteristics. The surface features control three major processes of dust production: the erosion threshold wind velocity, the wind shear-stress acting on the erodible surface, and the capability of the soil to release fine dust particles. Recently, many of dust emission schemes have been developed in order to provide an explicit representation of the mineral dust emission processes and the influence of surface features. These models are frequently classified according to their representation of mobilization. Two categories of models are distinguished (Zender et al., 2003). The simpler class, named the bulk mobilization schemes, calculates mobilization processes in terms of the third or fourth power of wind friction speed counting those of Tegen and Fung (1994), Mahowald et al. (1999), and Perlwitz et al. (2001). The complex class uses complete microphysical specification of the erodible environment to predict the saltation mass flux and resulting sandblasted dust emissions (Marticorena and Bergametti, 1995; Shao et al., 1996; Shao, 2001). These schemes have shown promising results at a regional scale (Shao and Leslie, 1997; Marticorena and al, 1997). Unfortunately, it's important to specify that many inputs for these fully microphysical schemes are not known. DEAD is an intermediate scheme in terms of complexity developed by Zender et al. (2003). The DEAD1.1.15 version used in Zender et al. (2003a) and Zender et al. (2003b) (http://dust.ess.uci.edu/dead/) was coupled with the externalised surface scheme SURFEX (Noilhan and Mahfouf, 1996) by Grini et al. (2006). This version assumes that the soil textures are globally uniform and are replete with particles

GMDD
4, 2893–2936, 2011

of a diameter of 75 µm (Zender et al., 2003). The saltation flux calculated for this type of particle is weighted with the fraction of sand available in the soil (Grini et al., 2006). The transfer function between the horizontal saltation flux and the vertical mass flux (α) is calculated by Marticorena and Bergametti (1995) relationships. DEAD use a uniform value of clay fraction ($M_{clay} = 0.2$) to determine the sandblasting mass efficiency α (Zender et al., 2003).

Nevertheless, some important processes able to influence dust emission are ignored in DEAD: geographic variation of surface size distribution (Marticorena et al., 1997) and size-dependent energy thresholds for particle released during sandblasting (Alfaro and Gomes, 2001). These limits can be performed in SURFEX scheme using the ECOCLIMAP database (Masson et al., 2003) providing information on the erodible fraction represented by the covers COVER004 and COVER005 relating to bare and rock soil and FAO database containing information on the sand and clay fractions allowing a classification of the soil textures (Masson et al., 2003). In this paper, a modification of the dust emission scheme (DEAD) is proposed and it consists of the introduction of geographic variation of surface size distribution, the Marticorena and Bergametti (1995) relationship in the horizontal saltation flux and the Shao (2001) formulation of sandblasting efficiency. To evaluate the performance of the modification introduced in the DEAD scheme, two experiments are produced in 0-D and 3-D with the old and the newly developed scheme. The 3-D experiment is realized within the atmospheric model ALADIN (Bubnová et al., 1995) coupled with surface scheme SURFEX. This experiment was run to simulate the 7–13 March west African dust storm. The results are compared with the local AOD and mass concentration measurements available from the AMMA database.

This paper is organised as follow: Sect. 2 summarizes the developed DEAD scheme which is introduced in SURFEX. Section 3 describes the 0-D and 3-D sensitivity and comparative study between the old and the new schemes. Section 4 presents concluding remarks with a summary of the main results.

GMDD
4, 2893–2936, 2011

2 Developed dust emission scheme coded in SURFEX

The representation of dust emission processes is very important in a dust model. It depends on wind conditions, soil characteristics and particle size. The developed dust emission scheme is based on parameterizations of soil aggregate saltation and sandblasting processes. The main steps for this scheme are: the calculation of soil aggregate size distribution for each model grid cell, the calculation of a threshold friction velocity leading to erosion and saltation processes, the calculation of the horizontal saltating soil aggregate mass flux, and finally the calculation of the vertical transportable dust particle mass fluxes generated by the saltating aggregates.

2.1 Soil texture methodology

Soil texture is the result of physicochemical processes acting on rocks and minerals (in situ or after transportation), influenced by external factors like climate, topography, and living organisms. The knowledge of the soil texture is necessary to determine the potential surface of the fine particles in the soil and to control the soil water contents. In order to characterize the erodible fraction of different types of soils, soil aggregate distributions are provided to the DEAD scheme. These distributions rely upon the USDA (United States Department of Agriculture) textural classification (Table 1), for which different types of soil are classified according to an index referring to the classic sand/clay/silt triangle of texture composition (Fig. 1) (Buckley, 2001). Sand particles range in size from 0.05–2.0 mm, silt ranges from 0.002–0.05 mm, and the clay fraction is made up of particles less than 0.002 mm in diameter. Gravel or rocks greater than 2 mm in diameter are not considered when determining texture. The combined portions of clay and sand in SURFEX scheme are provided by the global FAO database at 10 km resolution (Masson et al., 2003). These portions are showing, respectively, in Fig. 2a and b for the north Africa domain. Silt is the messing portion for having the sum of the three portions: sand, clay and silt that equals 1.

GMDD
4, 2893–2936, 2011

Once the sand, clay and silt percentages of a soil are known, the textural class can be read from the textural triangle. For example, a soil with 40 % sand, 40 % silt and 20 % clay would be classified as a loam. Therefore, a map of soil texture can be created (Fig. 3).

The analysis of Fig. 3 shows that, north Africa is dominated by a medium texture represented by loamy and sandy loam soil. These types of soil correspond to the Aridisols and Entisols in the Global soil region map classification (USDA/NRCS, 1999). In second position, we find sand and loamy sand soil, these soils correspond to shifting sands region in USDA classification (USDA/NRCS, 1999). This region, essentially constituted by a continuous substratum of coarse sands producing stable dunes made of coarse sands (median diameter 700 µm) and active dunes made of fine sands (median diameter 250 µm) (Callot et al., 2000). Silt loam occupies the major part of Hoggar and extreme eastern of Egypt toward red sea. Finally, clay and clay loam occupies very limited area in north Africa especially near Nil river and south-east of Sudan.

2.2 Soil aggregate distribution

A three-mode lognormal soil aggregate diameter distribution, $M(D_p)$, is related with each texture class following Zobler (1986):

$$\frac{dM(D_p)}{d\ln(D_p)} = \sum_{j=1}^{n} \frac{M_j}{\sqrt{2\pi}\ln(\sigma_j)} \exp \frac{\left(\ln D_p - \ln D_{med_j}\right)^2}{-2\ln^2\sigma_j} \quad (1)$$

where j refers to the mode, M_j is the relative weight of each mode j, D_{med_j} the geometric mean diameter, and σ_j the standard deviation in µm.

Table 2 shows the mass mean diameter (M_{med}), standard deviation (σ), and soil texture composition used to characterize each textural class (Zakey et al., 2006).

Following Marticorena and Bergametti (1995), the surface covered by each particle is assimilated to its basal surface. Thus a size distribution of the basal surface can

GMDD
4, 2893–2936, 2011

be computed from the mass distribution, assuming spherical particles with the same density ρ_p:

$$ds(D_p) = \frac{dM(D_p)}{\frac{2}{3}\rho_p D_p} \quad (2)$$

The total basal surface S_{total} is

$$S_{total} = \int_{D_p} dS(D_p)\, dD_p \quad (3)$$

and the normalized continuous relative distribution of basal surfaces dS_{rel}:

$$dS_{rel} = \frac{ds(D_p)}{S_p} \quad (4)$$

In our case, the potential of fine particles in the soil is represented by the relative surface occupied by each particle. In order to perform the model computation, we divide the all particles into four populations according to their size: (a) clay-size $D_p < 2\,\mu m$, (b) small silt-size $2\,\mu m < D_p < 10\,\mu m$, (c) large silt-size $10\,\mu m < D_p < 60\,\mu m$ and (d) sand-size $D_p > 60\,\mu m$ shows in Fig. 4 superposed with the cover COVER004.

The average relative surface for the named four populations represents the potential dust source emission (Fig. 5).

2.3 Dust mobilisation

The physical basis of the developed DEAD scheme is based globally on the Marticorena and Bergametti (1995) scheme (hereinafter referred to as MaB95), where dust is calculated as a function of saltation and sandblasting. We assume that the dust mobilisation starts when the friction velocity u_* exceeds a named threshold friction velocity u_{*t}. This last is parameterized following Marticorena and Bergametti (1995) and is obtained for a particle of diameter ($D_0 \approx 75\,\mu m$). Following MaB95, we assume all soils in

GMDD
4, 2893–2936, 2011

the erodable region contain particles of size D_0. The threshold friction velocity depends on drag partitioning (Marticorena and Bergametti, 1995) and soil moisture (Fécan et al., 1999).

Soil moisture generates a capillary force which is allowed to suppress dust deflation when the soil gravimetric water content (w) exceeds threshold soil moisture (w'). This threshold is defined in the developed DEAD scheme as following:

$$w' = b(0.17M_{\text{clay}} + 0.0014M_{\text{clay}}^2) \text{ and } 0.053 < w' < 0.15 \quad (5)$$

It was established, empirically, that setting $b = 3$ in Eq. (5) is better adapted to w predicted by the Interaction Soil Biosphere Atmosphere (ISBA) scheme (Noilhan and Planton, 1989) and provides a reasonable value of the erosion threshold velocity ratio compared with that obtained by Fécan et al. (1999).

The Owen effect is introduced as follow (Zender et al., 2003):

$$u_{*s} = u_* + 0.003\left(U_{10} - U_{10,\text{t}}\right)^2 \quad (6)$$

where u_{*s} is the corrected friction velocity due to the Owen effect and U_{10} , $U_{10,\text{t}}$ are, respectively, the wind speed and the threshold wind speed at 10 m.

In order to account for the soil aggregate distribution in the horizontal flux, the relation of Marticorena and Bergametti (1995) was chosen. This relation supposes that the contribution of each class size in the total flux depends directly on the relative surface occupied by each class in the soil. The total horizontal flux (G) is therefore the sum of the relative contributions of the various classes of sizes of particle considered (Marticorena and Bergametti, 1995):

$$G = aEc\frac{\rho}{g}u_*^3\int_{D_\text{p}}\left(1+\frac{u_{*\text{t}}}{u_*}\right)\left(1-\frac{u_{*\text{t}}^2}{u_*^2}\right)dS_{\text{rel}}(D_\text{p})dD_\text{p} \quad (7)$$

where E is the fraction of the erodable surface, a is the global mass flux tuning factor determined at posterior through the model experiments, $c = 2.61$, g is the gravitational

GMDD
4, 2893–2936, 2011

constant, ρ is the atmospheric density and $dS_{rel}(D_p)$ is the relative surface for each class size.

In our case we used four particles bins with a relative surface illustrated in Fig. 4.

To convert the horizontal flux (G) to vertical flux (F), DEAD adopts the Marticorena at al. (1995) formulation of sandblasting mass efficiency (α) with a constant value of clay fraction ($M_{clay} = 20\,\%$) (Zender et al., 2003). This relation provides a uniform value of α over all dust source emissions. Therefore, in the developed DEAD, the Shao et al. (1993) relationship was used for better representing the spatial variation of α.

$$\alpha = \frac{F}{G} = \frac{2}{3} \times \frac{\rho_p}{\rho} \times \frac{\beta \gamma g}{\left[u_{*t}(D_d)\right]^2} \tag{8}$$

$$\gamma = 2.5$$

and

$$\beta = \left[0.125 \times 10^{-4} \ln(D_s) + 0.328 \times 10^{-4}\right] \exp(-140.7.D_d + 0.37) \tag{9}$$

where D_d and D_s in mm and $\beta > 0$.

D_s: average diameter of the particles in saltation (~75 µm), D_d: average diameter of the suspended particles (~6.7 µm).

The vertical dust flux is partitioned into three modes following the AMMA parameterization (Crumeyrolle et al., 2011).

Dry deposition and sedimentation of dust aerosols are driven by the Brownian diffusivity and by gravitational velocity (see Tulet et al., 2005 and Grini et al., 2006 for details).

3 Sensitivity study: comparison between the developed DEAD version and the old scheme

In this section, a sensitivity study is conducted in order to show the performance and importance of the modifications introduced in DEAD scheme. This part of the study

GMDD
4, 2893–2936, 2011

contains two experiments: the first in 0-D and the second in 3-D where 7–13 March situations are simulated.

3.1 0-D simulations configurations

Different 0-D simulations presents the surface dust fluxes evolution depending on the friction velocity over a specific point, with the use of four different configurations of surface fluxes (EXP1, EXP2, EXP3 and EXP4) defined in Table 4. The goal of the EXP1 configuration is to show the influence of the Fécan (1999) formulation on the threshold friction velocity and to highlight the adapted Fécan formulation (Eq. 5) used in the developed DEAD scheme. The EXP2 configuration shows the consequences of the Marticorena and Bergametti (1995) formulation in the calculation of the sandblasting efficiency α when the variation of clay fraction in the ground from 0 to 20 %, is taken into account. The EXP3 configuration is the current version of DEAD used in SURFEX. Finally, the EXP4 configuration is the developed version of DEAD proposed in this paper. These configurations were tested for five types of soils in North Africa, namely: clay, loam, sandy loam, loamy sand and sand.

For all configurations the same erodable particle with diameter 75 µm is used and we consider the roughness length Z_0 for the bare ground constant and uniform, equal to 30 µm. The smooth roughness length Z_{0s} is given in the Table 4 with D_{med} being the median diameter for the coarser population of the soil size distribution in EXP4 case and finally the forcing soil wetness field is given by ISBA scheme. The results are exposed in Fig. 6.

3.1.1 Clay soil

Clay soil occupies a very limited area of the North African Sahara desert, particularly, at latitude 33° north between the Algerian and Tunisian border and extreme south-eastern Sudan between 12° and 15° latitude north. This soil contains over 40 % of clay. This substance acts as cement in the soil and fortifies the cohesion force. Over

GMDD
4, 2893–2936, 2011

this type of soil, the threshold friction velocity obtained by the EXP2, EXP3 and EXP4 configurations is 0.5 m s^{-1}, but the one obtained by EXP1 is more important: 0.6 m s^{-1}. Concerning surface fluxes, EXP1, EXP2 and EXP3, present the same sandblasting efficiency α and convergence in the evolution of the curves, depending on the friction velocity. In contrast, the EXP4 provides a very weak surface flux which does not exceed 1 µg m^{-2} s^{-1} .This underestimation is caused by the very low value of total relative surface of soil particles, which does not exceed 0.05, calculated for clay soil. In conclusion, EXP1, EXP2 and EXP3 show that the potential dust sources of clay soil are relatively weak, but EXP4 excluded it from the potential dust sources. It is true that the sandblasting efficiency is dependent on fine particles contained in the soil but also is controlled by large particles. Indeed, it is these particles which allow the release of fine particles while being activated by saltation. However, clay soil is very low in large particles and does not favor the saltation motion. It is then reasonable to obtain a low surface dust flux over this soil.

3.1.2 Loamy soils

Loamy soil is the dominant type of soil in the African Sahara desert, over this soil, EXP2, EXP3 and EXP4 start the dust emission at a friction velocity around 0.45 m s^{-1}, but the EXP1 starts at a friction velocity around 0.55 m s^{-1}. Concerning the surface fluxes, for a wind velocity less than 0.8 m s^{-1}, the evolution is nearly the same for the four representations. Beyond this velocity, the surface dust fluxes obtained with EXP1 and EXP3 are greater than those calculated with EXP2 and EXP4. In conclusion, the four representations find that loamy soil as a relatively moderate dust source emission.

3.1.3 Sandy loam soils

Sandy loam soil occupies the major part of northern Sudan and southern Egypt and Libya, a local part of the Bodélé depression, southern Niger and northern Mali and Mauritania. For these soils, the threshold friction velocity obtained by EXP2, EXP3 and

GMDD
4, 2893–2936, 2011

EXP4 is around 0.42 m s^{-1}, but EXP1 starts dust emission at a friction velocity around 0.5 m s^{-1}. Concerning surface fluxes, EXP1, EXP3 and EXP4 provide, relatively, the same surface dust fluxes. Opposition, EXP2 provides very weak surface dust fluxes. In conclusion, EXP1, EXP3 and EXP4 show that Sandy loam soil is a moderate dust emission source but EXP2 excludes it from the potential dust source. It can be seen that, the sandblasting efficiency is calculated in EXP2 by MaB95 for a varied clay fraction. For this type of soil, the percentage of clay is around 12 %, so the sandblasting efficiency ratio between this type of soil and that of soil with 20 % of clay is around 10, explaining the low value of this efficiency when taking into account the variation of clay in the ground.

3.1.4 Loamy sand soils

These soils occupy the large part of the Bodélé depression and a part of the Algerian and Nigerian border and a limited area in the Mauritanian and Algerian desert. Over loamy sand soil, EXP3 and EXP4 start dust erosion around 0.37 m s^{-1}, whereas EXP1 starts mobilisation around 0.48 m s^{-1}. As for surface fluxes, EXP1 and EXP3 present an important evolution of dust surface fluxes, whereas EXP4 presents a very important evolution of dust surface fluxes. On the other hand, EXP2 does not create significant dust surface fluxes as before with sandy loam soils. However, these soils are considered as the most important dust emission source in north Africa. Therefore, they are very well represented by EXP4 configuration.

3.1.5 Sand soils

These soils cover a large part of Mauritania and Niger, the eastern and western Great Erg of Algeria and a localized part of Egypt, Libya and Sudan. Over sand soil, EXP3 and EXP4 starts the dust mobilisation around 0.28 m s^{-1} but EXP1 begins mobilisation at a friction velocity around 0.43 m s^{-1}. As for surface fluxes, EXP1 and EXP3 provide very strong dust flux values and consider this soil the most important dust emission

GMDD
4, 2893–2936, 2011

sources. However, these soils have few fine particles and its aggregate is very coarse. In theory, these soils must provide low dust fluxes contrary to EXP1 and EXP3. On the other hand, EXP4 gives reasonable fluxes and classifies this soil after loamy sand and sandy loam in terms of source intensity.

3.1.6 Preliminary conclusions

Through this experiment we can conclude that the Fécan (1999) formulation provides very low threshold soil moisture. So, this threshold is often exceeded by soil moisture calculated by the ISBA scheme. Consequently, a correction of the threshold friction velocity is applied. That explains the important value of the threshold friction velocity obtained by EXP1 configuration over all soils.

The sandblasting efficiency calculated by the MaB95 formulation for a variable fraction of clay provides very low fluxes over Sandy loam, Loamy sand and Sandy soils, which is clarified in EXP2. These soil types cover the northern part of Sudan, the southern part of Egypt, the Bodélé depression, the large part of Mauritania, Mali, Niger and finally, the eastern and western Great Erg of Algeria. These zones are classified by some researches as potential dust source areas (Laurent et al., 2007), but they are ignored by the EXP2 configuration.

The DEAD (EXP3) and the developed DEAD configuration (EXP4) present the same threshold friction velocity. The minimum value is obtained for Sandy soil ($0.28\,m\,s^{-1}$). This value is in agreement with that obtained by (Marticorena et al., 1997) over this soil (7 to $8\,m\,s^{-1}$ at 10 m). Which explains the efficiency of the adapted Fécan (1999) formulation presented in Eq. (5). For surface fluxes, EXP3 presents uniform sandblasting efficiency for all soil types. Therefore, the only parameter which differentiated the potential dust sources is sand fraction (Fig. 2b). This configuration classified Sandy soil as first in terms of source intensity, second for Loamy sand soil, and in third position Sandy loam soil. However, it is noted that Sandy soil is constituted with coarse sand and has few fine particle. The assigned value of sandblasting efficiency α, by Marticorena et al. (1997) for similar types of soil is very low ($1.0 \times 10^{-7}\,cm^{-1}$). In another hand, the

GMDD
4, 2893–2936, 2011

EXP4 represents the potential dust source by the total average relative surface (Fig. 5) and classifies Loamy sand and Sandy loam as more important dust sources. These soils contain an important percentage of large particles supporting the movement by saltation and at the same time a sufficient percentage of fine particles ensures vertical release. Thus are very well represented by EXP4 configuration.

3.2 3-D Simulation; the 7–13 March case study

The 7–13 March dust storm represents an interesting case for studying dust aerosol impact in western Africa. This event is well described by Slingo et al. (2006) and Marticorena et al. (2010) and further analyzed by Tulet et al. (2008), Mallet et al. (2009), and Kocha et al. (2011). As described in Slingo et al. (2006), it was initiated by a cold front in the lee of the Atlas mountain that progressed southward and westward, producing dust emission all along its path. In this section, we simulate this event by using the previous configurations defined in Table 5 in order to illustrate the behaviour of each representation in three dimensions. EXP1 and EXP2 are fused into one configuration, THR, known as the theoretical version where we used the Fécan (1999) formulation to estimate the soil moisture effect and the MaB95 formulation to calculate the sandblasting efficiency α. EXP3 and EXP4 are samely represented in Table 5. The results are combined with available data from AMMA.

3.2.1 Model configuration and dust transport

The spectral hydrostatic atmospheric model ALADIN was used in this study. This model is developed in an international cooperation led by Météo France, operationally used for weather prediction. It is a fully, three-dimensional baroclinic system of primitive equations using a two-time-level semi-Lagrangian semi-implicit numerical integration scheme and a digital filter initialisation (Huth et al., 2003). The physical parameterization package comprises: gravity wave drag parameterization, semi-Lagrangian horizontal diffusion (SLDH), computed in spectral space, vertical diffusion and planetary

GMDD
4, 2893–2936, 2011

boundary layer parameterisation, sub-grid scale deep convection and convective precipitations, the RRTM scheme (Rapid Radiative Transfer Model) for long wave radiation (Mlawer et al., 1997) and Fouquart Morcrette for shortwave radiation have six spectral bands. The simple large-scale cloudiness and precipitation scheme was developed by Lopez (2002). For a complete scientific description, readers are refered to Bubnová et al. (1995), Radnóti (1995), Horányi et al. (1996), Geleyn (1998) and Váňa (1998).

Surface process are calculated by the externalized surface scheme (SURFEX) containing: the Interaction Soil Biosphere Atmosphere (ISBA) scheme (Noilhan and Planton, 1989), sea (Ecume fluxes), Town Energy Balance (TEB) (Masson, 2000) and lakes.

Dust aerosols are transported using the lognormal aerosol dynamic model ORILAM (Tulet et al., 2005).

The vertical diffusion of dust aerosols is calculated in ALADIN like temperature and moisture diffusion (Gibelin, 2004). Thus, the same exchange coefficient used for temperature and moisture is applied for dust aerosols.

The wet removal of dust aerosols is calculated using the SCAVenging submodel (Tost et al., 2006) developed for the MesoNH. For details of this formulation, refer to Tulet et al. (2010), Tost et al. (2006), and Berthet, et al. (2010).

The horizontal resolution of the ALADIN model version used in this study is 24 km centered over North Africa and 60 levels in the vertical; from the surface to 67 km. ALADIN is forced by the ARPEGE global model, which provides initial and lateral boundary conditions. In order to minimise spin up and establish reliable dust concentration conditions, the simulation is started from 1 March 2006 with a 48 h forecast with simulated dust concentration of the previous forecast used to initialise the dust concentration for the next model run.

3.2.2 Synoptic situation

The 7–13 March 2006 west African dust event was generated by a strong pressure gradient over western Africa between 7 to 9 March (Fig. 7). The 850 hPa geopotential

GMDD
4, 2893–2936, 2011

field from 8 March at 12:00 UTC, forecasted by ALADIN (Fig. 7b), shows high pressure over Mauritania and low pressure over Libya. This strong geopotential gradient generate an intense surface Harmattan flux over northern Niger and Chad ($15\,m\,s^{-1}$), northern Mali ($12\,m\,s^{-1}$) and Mauritania ($12\,m\,s^{-1}$) (Fig. 7a). This strong surface winds led, during the 7–13 March period, an intense dust storm which was readily observed from the MSG-SEVIRI satellite images (Schmetz et al., 2006; Slingo et al., 2006) on 8 March, at 12:00 UTC (Fig. 8). A high dust plume is observed spreading from the desert regions of Mali, Niger and Chad to the southwest part of the domain. The evolution of the AOD (at 550 nm) has been observed by the AQUA-MODIS satellite (Fig. 9a, c and e). These data have been obtained from the MODIS on line visualization and Analysis System (MOVAS) tool, developed at NASA (http://disc.sci.gsfc.nasa.gov/giovanni#maincontent). On 8 March, (Fig. 9a), we can observe that the dust plumes does not reach the Guinea Gulf and is still located north of Benin and central of Nigeria. On 10 March, it is interesting to note that the AQUA-MODIS satellite also retrieved three AOD maxima exceeding 3 in the same location around Nigeria (Fig. 9c). On 12 March, the AQUA-MODIS observed high AOD over Benin, Nigeria and Cameroon exceeding 3 in the coastal regions (Fig. 9e).

The evolution of the AOD (at 550nm) for Sahelian dust simulated by ALADIN (Fig. 9b, d and f) showed a strong band of high AOD appearing from Chad to Senegal on 8 March. Different AOD maxima were simulated in Chad (3), the southern part of Niger, northern Nigeria (3.4) and Senegal (3) (Fig. 9b) which are in agreement with that observed by AQUA-MODIS. On the other hand, we indicate the delay of the initiation of dust event at Capo Verde, Djougou and Ilorin. On 10 March (Fig. 9d), the dust plume spread to the South, reaching the Gulf of Guinea. In particular, three maximums of AOD were simulated: the first maximum is around 3, was simulated above Nigeria (from Benin to southern Chad and Cameroon), the second and the third maximums are around 2.6 and were simulated respectively, over Mali and western of Senegal toward Atlantic Ocean. On 12 March, the intense dust plume continued its extension to the south over the Guinea Sea and the Atlantic Ocean but decreased over the whole

GMDD
4, 2893–2936, 2011

domain (Fig. 9f). It is interesting to note that the coupled system ALADIN-SURFEX reproduced the dust storm event in intensity and location satisfactory.

3.2.3 Temporal evolution of AOD between 1 and 15 March 2006

The simulated AOD between 1 and 15 March 2006 are compared to in situ AERONET photometer measurements located at: Banizoumbou (Niger) and DMN Meine Soroa (Niger), to control the dust source emission, Mbour (Senegal) and Capo Verde, to control the western transport towards the Atlantic Ocean, Djougou (Benin) and Ilorin (Nigeria), to control the southern transport towards Guinea Golf, and finally, Cairo(Egypt) and Tamanrasset (Algeria) were to supplement data. The results are illustrated in Fig. 10 where the observed AOD are represented by blue dots, the THR, EXP3 and EXP4 are represented respectively by a red line, green line and black line.

Banizoumbou and Soroa mark the closed dust source towards southern North Africa with Sandy loam soil type. During the dust storm event, these two regions are fed, simultaneously, by the local dust source and the Harmattan dust flux. Over these two stations, investigation of the AOD observation shows that the dust storm event started on 7 March and ended on 11 March (Fig. 10a and b). The maximum AOD is observed on 8 March reaching 4.2 over Banizoumbou and that observed over Soroa is on 9 March and reached 4.3. After 11 March AOD decreased and became less than 1. Concerning simulated AOD, EXP3 and EXP4 start dust ascension in agreement with the observations, especially over Soroa, but over Banizoumbou a difference in intensity is notable. On 9 and 10 March, the AOD simulated over Banizoumbou with EXP3 reached 3.5, but the observations do not exceed 2.8. Whereas, EXP4 predicts AOD in agreement with observations on 9 March (2.8) but on 10 March the predicted value of AOD is slightly over the estimate (2.6). On the other hand, the AOD simulated by THR is largely underestimated and did not exceed 1 during the dust storm event.

Mbour and Capo Verde are affected by the dust aerosols transported toward western Africa and the Atlantic Ocean. Over these two stations the maximum observed AOD is seen on 9 March and exceeded 2.5 (Fig. 10c and d). However, EXP3 predicts a peak

GMDD
4, 2893–2936, 2011

of AOD exceeding 5 over Mbour, at 9 March but that predicted by EXP4 at the same time is in agreement with the observations. To understand this anomaly and its origin, a reproduction of the trajectory of the air mass was made with the NOAA Hysplit model at level 500 m level (red line), 1000 meter level (blue line) and 3000 m level (green line) (Fig. 11a). This figure shows that the trajectory of the air mass overflowing Mauritania and Mali. These regions are covered with sandy soil and considered by EXP3 as an important dust source emission but only a moderate source for EXP4. For THR, we note that simulated AOD is underestimated during the dust storm event.

Djougou and Ilorin are affected by the northern flux that transport dust aerosols toward the Guinea Golf. The registered AOD shows that the dust plum reaches Djougou on 8 March (Fig. 10e), where we register AOD is greater than 1, but Ilorin is affected on 10 March, (Fig. 10f). The NOAA Hysplit model trajectory (Fig. 11b) shows that the air mass trajectory ended over Djougou at 10 March coming from the south, the Atlantic Ocean and Guinea Golf in surface and mean altitude (red and blue line) and is saturated by salt aerosols. However, these aerosols are weakly diffused, and less influence the AOD. On the other hand, at higher altitude (green line) the trajectory came from northeast, sweeping through the center of Niger, northern Nigeria, which was already affected by the dust storm between 8 and 10 March. During this period, Aladin simulated this transport with delay and underestimate the AOD. Between 11 to 14 March, the observed AOD over Djougou exceeded 2 and then decreased after 14 March These AOD are very well predicted by EXP3 and EXP4 except on 13 March, where EXP3 overestimated the AOD. Over Ilorin, strong AOD are observed between these days, with a maximum exceeding 4 on 11 March. These AOD are underestimated by the EXP3 representation as in the study of Tulet et al. (2008) but EXP4 forecast reached 4 on 11 March.

Over Cairo (Fig. 10g), there were two episodes for the dust event. The first, on 7 March to 9 March, when AOD observed attained a value of 1.7 on 8 March. The second episode is observed on 13 March. These episodes are very well simulated by EXP3 and EXP4 representations, but they are not taken into account by the THR

GMDD
4, 2893–2936, 2011

configuration. Over Tamanrasset (Fig. 10h), the AOD simulated are weak and are in agreement with the observations.

To summarize, dust storm events are well simulated globally by EXP3 and EXP4. In terms of intensity, we note that, EXP4 reproduced well the AOD values, especially over Mbour, Djougou and Ilorin but over Soroa, Cairo and Tamanrasset they are converged. In terms of extension and transport, we registered for both configurations a delay in the transport of dust aerosols for remote stations from the dust sources in particular Capo Verde for the western transport and Djougou for the southern transport. It is interesting to signal that the three parameterizations missed the beginning of the dust event over Banizoumbou, and also the bad simulated AOD by THR over all stations during the dust storm event.

3.2.4 Temporal evolution of dust surface concentration between 1 and 15 March 2006

The evolution of dust surface concentration over Banizoumbou and Mbour between 1 and 15 March simulated by ALADIN, with the three previous dust emission configurations are compared with the observations. The results are shown in Fig. 12.

Over Banizoumbou (Fig. 12a), the dust surface concentrations observed are important during the dust storm event with a maximum reaching 4500 $\mu g\,m^{-3}$ at 9 March. 7 March shows the beginning of this episode with one observation of magnitude 2500 $\mu g\,m^{-3}$, but those simulated by EXP3 and EXP4 are under 1000 $\mu g\,m^{-3}$. The second peak is observed on 8 March and reached 3500 $\mu g\,m^{-3}$, which is well simulated by EXP3, but EXP4 underestimates this peak. The third peak, that is the maximum (4500 $\mu g\,m^{-3}$), is seen on 9 March. This peak is very well simulated by EXP4 whereas it is overestimated by EXP3. During this episode the THR is deeply underestimates the dust concentration. After 10 March, EXP3 largely overestimates the concentration so that EXP4 is in agreement with the observations.

Over Mbour (Fig. 12b), during the dust storm event, the THR configuration underestimates the surface concentration. 8 March shows the beginning of the episode over

GMDD
4, 2893–2936, 2011

Mbour, where a peak around 1500 $\mu g\,m^{-3}$ was observed, therefore EXP4 predicts a peak around 2500 $\mu g\,m^{-3}$ and EXP3 predicts a very high peak around 5000 $\mu g\,m^{-3}$. The second peak around 2500 $\mu g\,m^{-3}$ is observed on 9 March and is very well predicted by EXP4 but it is overestimated by EXP3. After 10 March, EXP4 is in good agreement with the observations but EXP3 overestimates the surface concentration.

3.2.5 Surface dust flux

In this section, a comparison of 48 h accumulated dust flux is made, simulated by EXP3 (Fig. 13a and c) and EXP4 (Fig. 13b and d) between 7–9 March and 9–11 March 2006 at 00:00 UTC. The lack of surface dust flux observations leads us, in this comparison study, to provide only the difference between these two configurations in terms of spatial repartition and intensity. First, In terms of repartitioning, we observe that the region of dust emission provided by EXP3 is larger than the one obtained by EXP4, especially on 7–9 March where EXP3 shows a continuous spatial field of dust flux over Libya, western of Egypt, northern of Niger, Mali and Mauritania, but that obtained by EXP4 is scattered and sometimes very large. In terms of intensity, the accumulated dust flux intensity obtained by EXP3 and EXP4 largely depends on the region and is banded to the dust source emission represented previously. Between 7–9 March, EXP3 predict 3 important cores of dust flux (30–36 $g\,m^{-2}$), all located over Sandy soil, in north-eastern Libya and Niger and in the center of Niger, but EXP4 predicted one small core located in north-eastern Niger. On 9–11 March EXP3 predicted one intense core of dust flux located at the Bodélé depression (30–36 $g\,m^{-2}$) but the one obtained by EXP4 is very intense (40–45 $g\,m^{-2}$). That is more in agreement with climatology data for these regions and literature studies (Laurent et al., 2008).

GMDD
4, 2893–2936, 2011

4 Conclusions

Through this work, a contribution was made to the development of the ALADIN model by introducing atmospheric dust aerosol as a prognostic tracer in the model. The production and emission phases are simulated in the ISBA scheme which is integrated in SURFEX. To improve the dust emission in SURFEX, the dust emission scheme (DEAD) was developed, by introducing the geographic variation of the surface size distribution, the Marticorena and Bergametti (1995) relationship in the horizontal saltation fluxes and the Shao (2001) formulation in the calculation of the sandblasting efficiency. These modifications and changes will have entered in the next version of SURFEX SURFEX7.1 (http://www.cnrm.meteo.fr/surfex/). The comparative study conducted in 0-D showed that the moisture effect introduced by the Fécan formulation provides low threshold moisture, then generates an important erosion threshold over all soils. The MaB95 formulation provides weak sandblasting efficiency, particularly over Loamy sand and Sandy loam soils. However, these soils are considered by some authors as an important dust source. Indeed Marticorena et al. (1997) used data from Chatenet et al. (1996) and Gillette (1979) to estimate the size distribution and fine particle content in the soil. These data were different from the FAO data base and there is no correspondence between the fines particle used in MaB95 and the clay content provided by the FAO data used in DEAD. On the other hand, the developed DEAD scheme reproduced the localization of the dust source emission and the erosion thresholds satisfactory. This scheme emphasizes loamy sand soil and sandy loam soil as important dust source. These soils contain, at the same time, large particles supporting the saltation and fine particles available for the suspension. This mixture of particles helps the sandblasting phenomena.

The second part of the paper was dedicated to a 3-D evolution of the dust distribution using the coupled system ALADIN-SURFEX. The 7–13 March West African dust storm were simulated using three representations of the dust emission scheme, theoretical (THR), DEAD, and finally the developed DEAD scheme which was presented in this

GMDD
4, 2893–2936, 2011

paper. The results showed that the theoretical representation always underestimates the AOD and concentrations over all photometer AERONET stations. This underestimation is caused by the incompatibility of the theoretical formulation within FAO and ECOCLIMAP databases used in the SURFEX scheme. On the other hand, DEAD and developed DEAD representations provided generally reasonable AOD and began the dust storm event as observed. Therefore, the threshold friction velocity calculated with the arranged Fécan formulation is accurate. Unfortunately, DEAD largely overestimated the concentrations at the surface. This overestimation is due to the strong uniform sandblasting efficiency calculated with a clay fraction equal to 20 %for all soils types. On the other hand, the developed DEAD scheme provide very satisfactory surface concentrations and rigorously identified the natural dust sources. These results justify the correct choice of the formulations used in this scheme and the representativeness of the natural dust sources by the relative surfaces.

Acknowledgements. The authors thank F. Ounnar (Director General of the Algerian Met Office), C. Fischer (LTM ALADIN/France) and B. Hamadache (Director of Forecasting). This work was supported by Algerian Met Office (ONM), Météo France, Centre National de Recherches Météorologiques (CNRM) and the French Embassy in Algeria.

References

Alfaro, S. C. and Gomes, L.: Modeling mineral aerosol production by wind erosion: Emission intensities and aerosol distributions in source areas, J. Geophys. Res, 106, 18075–18084, 2001.

Bagnold, R. A.: The Physics of Blown Sand and Desert Dunes, Methuen, New York, 265 pp., 1941.

Berthet, S., Leriche, M., Pinty, J.-P., Cuesta, J., and Pigeon, G.: Scavenging of aerosol particles by rain in a cloud resolving model, Atmos. Res., 96, 325–336, 2010.

Bubnová, R., Hello, G., Bénard, P., and Geleyn, J. F.: Integration of the fully elastic equations cast in the hydrostatic pressure terrain following coordinate in the framework of the ALADIN NWP system, Mon. Weather Rev., 123, 515–535, 1995.

GMDD

4, 2893–2936, 2011

Buckley, R. L.: Spatial Variation of Soil Type and Soil Moisture in the Regional Atmospheric Modeling System (U), WSRC-TR 2001-00119 (U), Savannah River Technology Center, Westinghouse Savannah River Company, Aiken, SC 29808, doi:10.2172/782676, 2001.
Callot, Y., Marticorena, B., and Bergametti, G.: Geomorphologic approach for modelling the surface features of arid environments in a model of dust emission: application to the Sahara desert, Geodin. Acta, 13, 245–270, 2000.
Chatenet, B., Marticorena, B., Gomes, L., and Bergametti, G.: Assessing the size distribution of desert soils erodible by wind, Sedimentology, 43, 901–911, 1996.
Crumeyrolle, S., Tulet, P., Gomes, L., Garcia-Carreras, L., Flamant, C., Parker, D. J., Matsuki, A., Formenti, P., and Schwarzenboeck, A.: Transport of dust particles from the Bodélé region to the monsoon layer- AMMA case study of the 9-14 June 2006 period, Atmos. Chem. Phys., 11, 479–494, doi:10.5194/acp-11-479-2011, 2011.
Fécan, F., Marticorena, B., and Bergametti, G.: Parametrization of the increase of the aeolian erosion threshold wind friction velocity due to soil moisture for arid and semi-arid areas, Ann. Geophys., 17, 149–157, doi:10.1007/s00585-999-0149-7, 1999.
Foret, G., Bergametti, G., Dulac, F., and Menut, L.: An optimized particle size bin scheme for modelling mineral dust aerosol, J. Geophys. Res., 111, D17310, doi:10.1029/2005JD006797, 2006.
Geleyn, J. F.: Adaptation of spectral methods to non-uniform mapping (global and local), ECMWF Seminar Proceedings on "Recent developments in numerical methods for atmospheric modeling", 7–11 September 1998, 226–265, 1998.
Gibelin, A. L.: Externalisation du schéma de surface Isba du modèle de circulation générale Arpège-Climat, Note de Centre du GMGEC no. 88, 2004.
Gillette, D. A.: Environmental factors affecting dust emission by wind erosion in Saharan dust, edited by: Morals, C., John Wiley, New York, 71–94, 1979.
Greeley, R. and Iversen, J. D.: Wind as a Geological Process, Cambridge Univ. Press, New York, 1985.
Grini, A., Tulet, P., and Gomes, L.: Dusty weather forecasts using the MesoNH mesoscale atmospheric model, J. Geophys. Res., 111, D19205, doi:10.1029/2005JD007007, 2006.
Horányi, A., Ihàsz, I., and Radnoti, G.: ARPEGE/ALADIN: A numerical weather prediction model for Central Europe with the participation of the Hungarian Meteorological Service, idöjàràs, 100, 277–301, 1996.
Huth, R., Mlàdek, R., Metelka, L., Sedlàk, P., Huthová, Z., Kliegrová, S., Kysely, J., Pokorná,

GMDD
4, 2893–2936, 2011

L., Halenka, T., and Janousek, M.: On the integrability of limited-area numerical weather prediction model ALADIN over extended time periods, Stud. Geophys. Geod., 47, 863–873, 2003.

Kocha, C., Lafore, J.-P., Tulet, P., and Seity, Y.: High-resolution simulation of a major West African dust-storm: comparison with observations and investigation of dust impact, Q. J. Roy. Meteorol. Soc., doi:10.1002/qj.927, 2011.

Iversen, J. D. and White, B. R.: Saltation threshold on Earth, Mars and Venus, Sedimentology, 29, 111–119, 1982.

Laurent, B., Marticorena, B., Bergametti, G., Léon, J. F., and Mahowald, N. M.: Modeling mineral dust emission from the sahara desert using new surface properties and soil database, J. Geophys. Res., 113, D14218, doi:10.1029/2007JD009484, 2008.

Lopez, P.: Implementation and validation of a new prognostic large-scale cloud and precipitation scheme for climate and data-assimilation purposes, Q. J. R. Meteorol. Soc., 128, 229–257, 2002.

Mahowald, N., Kohfeld, K., Hansson, M., Balkanski, Y., Harrison, S. P., Printice, I. C., Schulz, M., and Rodhe, H.: Dust sources and deposition during the last glacial maximum and current climate: A comparison of model results with paleodata from ice cores and marine sediments, J. Geophys. Res., 104, 15895–15916, 1999.

Mahowald, N. M., Baker, A. R., Bergametti, G., Brooks, N., Duce, R. A., Jickells, T. D., Kubilay, N., Prospero, J. M., and Tegen, I.: Atmospheric global dust cycle and iron inputs to the ocean, Global Biogeochem. Cy., 19, GB4025, doi:10.1029/2004GB002402, 2007.

Mallet, M., Tulet, P., Sera, D., Solmon, F., Dubovik, O., Pelon, J., Pont, V., and Thouron, O.: Impact of dust aerosols on the radiative budget, surface heat fluxes, heating rate profiles and convective activity over West Africa during March 2006, Atmos. Chem. Phys., 9, 7143–7160, doi:10.5194/acp-9-7143-2009, 2009.

Marticorena, B. and Bergametti, G.: Modeling the atmospheric dust cycle: 1. Design of a soil-derived dust emission scheme, J. Geophys. Res., 100, 415–416, 1995.

Marticorena, B. and Bergametti, G.: Two year simulations of seasonal and interannual changes of the Saharan dust emissions, Geophys. Res. Lett., 23, 1921–1924, 1996.

Marticorena, B., Bergametti, G., Aumont, B., Callot, Y., N'Doume, C., and Legrand, M.: Modeling the atmospheric dust cycle: 2. Simulation of the Saharan dust sources, J. Geophys. Res., 102, 4387–4404, 1997a.

Marticorena, B., Bergametti, G., Gillette, D. A., and Belnap, J.: Factors controlling threshold

GMDD

4, 2893–2936, 2011

friction velocity in semiarid and arid areas of the United States, J. Geophys. Res., 102, 277–23, 1997b.
Marticorena, B., Kardous, M., Bergametti, G., Callot, Y., Chazette, P., Khatteli, H., Le Hégarat-Mascle, S., Maillé, M., Rajot, J. L., Vidal-Madjar, D., and Zribi, M.: Surface and aerodynamic roughness in arid and semiarid areas and their relation to radar backscatter coefficient, J. Geophys. Res., 111, F03017, doi:10.1029/2006JF000462, 2006.
Marticorena, B., Chatenet, B., Rajot, J. L., Traoré, S., Coulibaly, M., Diallo, A., Koné, I., Maman, A., NDiaye, T., and Zakou, A.: Temporal variability of mineral dust concentrations over West Africa: analyses of a pluriannual monitoring from the AMMA Sahelian Dust Transect, Atmos. Chem. Phys., 10, 8899–8915, doi:10.5194/acp-10-8899-2010, 2010.
Martin, J. H.: Glacial-interglacial CO_2 change: The iron hypothesis, Paleoceanography, 5, 1–13, 1990.
Masson, V.: A physically-based scheme for the urban energy balance in atmospheric models, Bound.-Lay. Meteorol., 94, 357–397, 2000.
Masson, V., Champeaux, J., Chauvin, F., Meriguet, C., and Lacaze, R.: A global database of land surface parameters at 1-km resolution in meteorological and climate models, J. Climate, 16, 1261–1282, 2003.
Mlawer, E. J., Taubman, S. J., Brown, P. D., Iacono, M. J., and Clough, S. A.: RRTM, a validated correlated-k model for the longwave, J. Geophys. Res., 102, 16663–16682, 1997.
Morcrette, J. and Fouquart, Y.: The overlapping of cloud layers in shortwave radiation parameterizations, J. Atm. Sci. , 43, 321–328, 1986.
Nicholson, S. E., Tucker, C. J., and Ba, M. B.: Desertification, drought, and surface vegetation: An example from the West African Sahel, Bull. Am. Meteorol. Soc., 79, 815–829, 1998.
Nickovic, S. and Dobricic, S.: A model for long-rang transport of desert dust, Mon. Weather Rev., 124, 2537–2544, 1996.
Nickovic, S., Kallos, G., Papadopoulos, A., and Kakaliagou, O.: Model for prediction of desert dust cycle in the atmosphere, J. Geophys. Res., 106, 18113–18129, 2001.
Noilhan, J. and Mahfouf, J. F.: The ISBA land surface parameterization scheme., Glob. Planet Change, 13, 145–159, 1996.
Noilhan, J. and Planton, S.: A simple parameterization of land surface processes for meteorological models, Mon. Weather Rev. 117, 536–549, 1989.
Perlwitz, J., Tegen, I., and Miller, R. L.: Interactive soil dust aerosol model in the GISS GCM: 1. Sensitivity of the soil dust cycle to radiative properties of soil dust aerosols, J. Geophys.

GMDD
4, 2893–2936, 2011

Res., 106, 18167–18192, 2001.
Prospero, J. M.: Long-term measurements of the transport of African mineral dust to the southeastern United States: Implications for regional air quality, J. Geophys. Res., 104, 15917–15928, 1999.
Radnóti, G.: Comments on "A spectral limited-area formulation with time-dependent boundary conditions applied to the shallowwater equations". Mon. Weather Rev., 123, 3122–3123, 1995.
Shao, Y.: A model for mineral dust emission, J. Geophys. Res., 106, 20239–20254, 2001.
Shao, Y. and Leslie, M.: Wind erosion prediction over the Australian continent, J. Geophys. Res., 102, 30091–30105, 1997.
Shao, Y. and Lu, I.: A simple expression for wind erosion threshold friction velocity, J. Geophys. Res., 105, 22437–22443, 2000.
Shao, Y., Raupach, M. R., and Findlater, P. A.: Effect of saltation bombardment on the entrainment of dust by wind, J. Geophys. Res., 98, 12719–12726, 1993.
Shao, Y., Raupach, M. R., and Leys, J. F.: A model for predicting aeolian sand drift and dust entrainment on scales from paddock to region, Aust. J. Soil Res., 34, 309–342, 1996.
Shao, Y., Yang, Y., Wang, J., Song, Z., Leslie, L. M., Dong, C., Zhang, Z., Lin, Z., Kanai, Y., Yabuki, S., and Chun, Y.: Northeast Asian dust storms: Real-time numerical prediction and validation, J. Geophys. Res., 108, 4691, doi:10.1029/2003JD003667, 2003.
Slingo, A., Ackerman, T. P., Allan, R. P., Kassianov, E. I., McFarlane, S. A., Robinson, G. J., Barnard, J. C., Miller, M. A., Harries, J. E., Russell, J. E., and Dewitte, S.: Observations of the impact of a major Saharan dust storm on the atmospheric radiation balance, Geophys. Res. Lett., 33, L24817, doi:10.1029/2006GL027869, 2006.
Swap, R., Garstang, M., Greco, S., Talbot, R., and Kallberg, P.: Saharan dust in the Amazon Basin, Tellus, Ser. B, 44, 133–149, 1992.
Tegen, I. and Fung, I.: Modeling of mineral dust in the atmosphere: Sources, Transport, and optical thickness, J. Geophys. Res., 99, 22897–22914, 1994.
Tegen, I., Lacis, A. A., and Fung, I.: The influence on climate forcing of mineral aerosols from disturbed soils, Nature, 380, 419–422, 1996.
Tegen, I., Heinold, B., Todd, M., Helmert, J., Washington, R., and Dubovik, O.: Modelling soil dust aerosol in the Bodélé depression during the BoDEx campaign, Atmos. Chem. Phys., 6, 4345–4359, doi:10.5194/acp-6-4345-2006, 2006.
Tulet, P., Crassier, V., Cousin, F., Suhre, K., and Rosset, R.: ORILAM, a three-moment log-

GMDD
4, 2893–2936, 2011

normal aerosol scheme for mesoscale atmospheric model: Online coupling into the Meso-NH-C model and validation on the Escompte campaign, J. Geophys. Res., 110, D18201, doi:10.1029/2004JD005716, 2005.

Tulet, P., Mallet, M., Pont, V., Pelon, J., and Boon, A.: The 7–13 March 2006 dust storm over West Africa: Generation, transport, and vertical stratification, J. Geophys. Res., 113, D00C08, doi:10.1029/2008JD009871, 2008.

Tulet, P., Crahan_Kaku, K., Leriche, M., Aouizerats, B., and Crumeyrolle, S.: Mixing of dust aerosols into a mesoscale convective system Generation, filtering and possible feedbacks on ice anvils, Atmos. Res., 96, 302–314, 2010.

United States Department of Agriculture (USDA), Natural Resources Conservation Service (NRCS), Soil Taxonomy: A Basic System of Soil Classification for Making and Interpreting Soil Surveys Agr. Handb., US Govt Print Office, Washington DC, 20402, 2nd Edn., 436 pp., 1999.

Váňa, F.: Physical parameterizations in the ALADIN model, Meteorol. zpr., 51, 33–44, 1998.

Zakey, A. S., Solmon, F., and Giorgi, F.: Implementation and testing of a desert dust module in a regional climate model, Atmos. Chem. Phys., 6, 4687–4704, doi:10.5194/acp-6-4687-2006, 2006.

Zender, C. S., Bian, H., and Newman, D.: Mineral Dust Entrainment and deposition (DEAD) model: Description and 1990s dust climatology, J. Geophys. Res., 108, 4416, doi:10.1029/2002JD002775, 2003.

Zobler, L.: A World soil file for global climate modelling, Tech. Rep. NASA-TM-87802, 32 pp., 1986.

GMDD

4, 2893–2936, 2011

Table 1. Soil texture classification following USDA (1998).

	Soil texture		Soil Texture
1	Sand	7	Silty clay loam
2	Loamy sand	8	Clay loam
3	Sandy loam	9	Sandy clay
4	Silt loam	10	Silty clay
5	Loam	11	Clay
6	Sandy clay loam	12	Silt

GMDD
4, 2893–2936, 2011

Table 2. The 12 basic USDA soil texture indices and corresponding soil aggregate size distribution parameters.

	Mode 1			Mode 2			Mode 3		
soil type	%	D_{med}	σ	%	D_{med}	σ	%	D_{med}	σ
Sand	90	1000	1.6	10	100	1.7	0	10	1.8
Loamy sand	60	690	1.6	30	100	1.7	10	10	1.8
Sandy loam	60	520	1.6	30	100	1.7	10	5	1.8
Silt loam	50	520	1.6	35	100	1.7	15	5	1.8
Loam	35	520	1.6	50	75	1.7	15	2.5	1.8
Sandy clay loam	30	210	1.7	50	75	1.7	20	2.5	1.8
Silt clay loam	30	210	1.7	50	50	1.7	20	2.5	1.8
Clay loam	20	125	1.7	50	50	1.7	30	1	1.8
Sandy clay	65	100	1.8	0	10	1.8	35	1	1.8
Silty clay	60	100	1.8	0	10	1.8	40	0.5	1.8
Clay	50	100	1.8	0	10	1.8	50	0.5	1.8
Silt	45	520	1.6	40	75	1.7	15	2.5	1.8

GMDD
4, 2893–2936, 2011

Table 3. The upper air dust modes in function of mass fraction M_i , diameter D_i(µm) and standard deviation σ_i.

	Mode 1	Mode 2	Mode 3
Mass fraction M_i	0.0008	0.0092	0.99
D_i (µm)	0.078	0.641	5.00
σ_i	1.75	1.76	1.70

GMDD
4, 2893–2936, 2011

Table 4. Definition of the four configurations tested for five types of soils.

Compared elements	EXP1	EXP 2	EXP 3	EXP 4
Geographic size distribution	Uniform texture	Uniform texture	Uniform texture	USDA 1998 textures
Moisture effect	Fécan (1999)	Fécan (1999) with w' is given by Eq. (5)	Fécan (1999) with w' is given by Eq. (5)	Fécan (1999) with w' is given by Eq. (5)
Drag partitioning effect	$Z_{0s} = 33.3\,\mu m$ DEAD	$Z_{0s} = 33.3\,\mu m$ DEAD	$Z_{0s} = 33.3\,\mu m$ DEAD	$Z_{0s} = D_{med}/30\,\mu m$ MaB95
Saltation fluxes	White (1979)	White (1979)	White (1979)	MaB95
$\alpha = F/G$	MaB95 with $M_{clay} = 20\,\%$	MaB95 with $0 < M_{clay} < 20\,\%$	MaB95 with $M_{clay} = 20\,\%$	Shao (1993)
Dust source intensity	M_{sand}	M_{sand}	M_{sand}	Relatives surface dS_{rel} for each population

GMDD
4, 2893–2936, 2011

Importance of the surface size distribution of erodible material

M. Mokhtari et al.

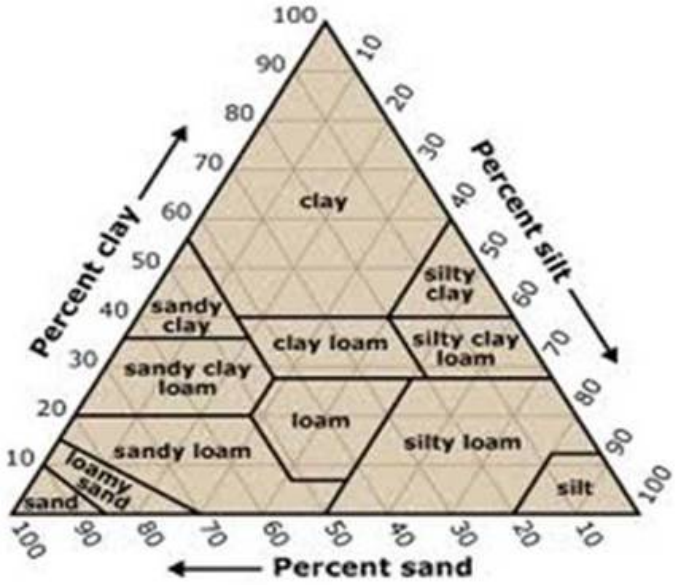

Fig. 1. Sand/clay/silt triangle of texture composition according USDA (1998).

GMDD
4, 2893–2936, 2011

Importance of the surface size distribution of erodible material

M. Mokhtari et al.

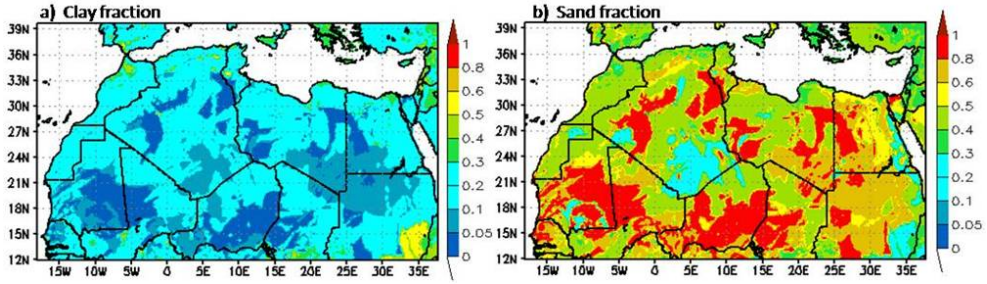

Fig. 2. Percentage of clay **(a)** and sand **(b)** for North Africa according FAO databases.

GMDD
4, 2893–2936, 2011

Importance of the surface size distribution of erodible material

M. Mokhtari et al.

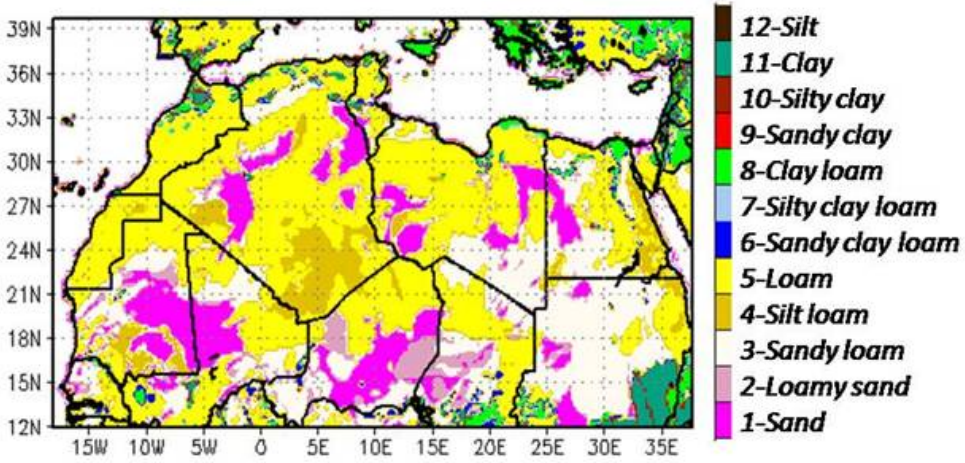

Fig. 3. Soil texture map for north Africa obtained by combining sand/clay/silt USDA textural triangle and clay, sand portion provided by FAO databases.

GMDD
4, 2893–2936, 2011

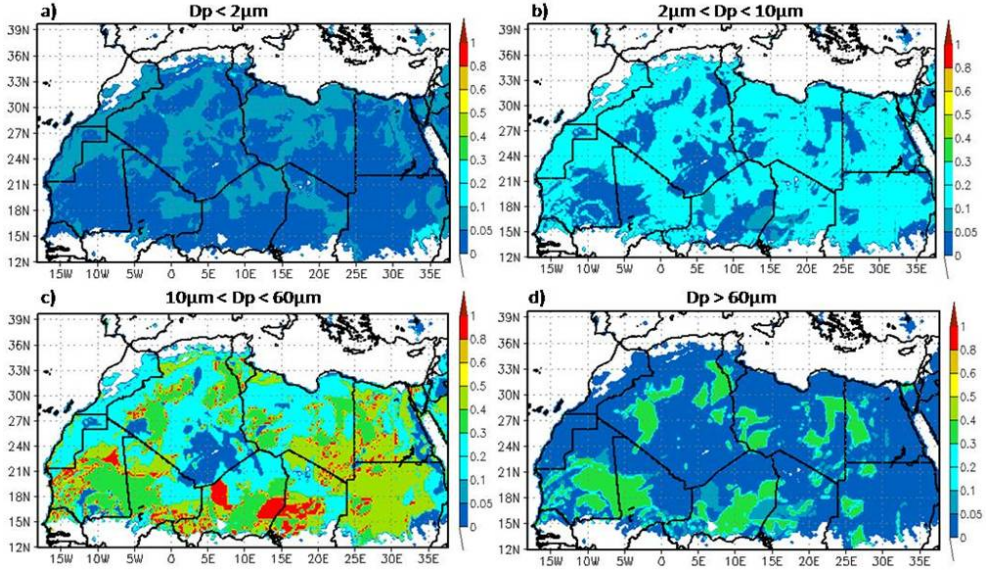

Fig. 4. The average relative surface for each population of soil particle with diameter comprised: **(a)** D_p <2 µm, **(b)** 2 µm < D_p < 10 µm, **(c)** 10 µm < D_p < 60 µm, and **(d)** D_p > 60 µm.

GMDD
4, 2893–2936, 2011

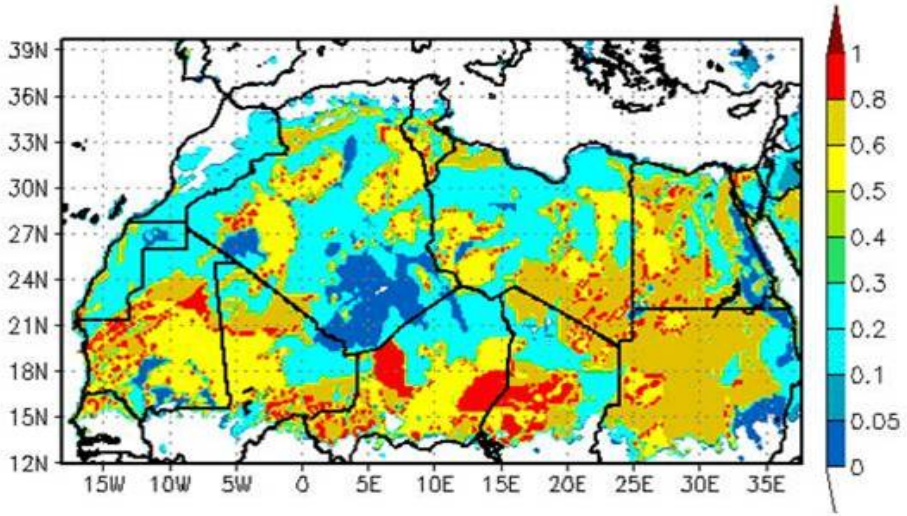

Fig. 5. Total average relative surface for the four populations of particles over north Africa.

GMDD
4, 2893–2936, 2011

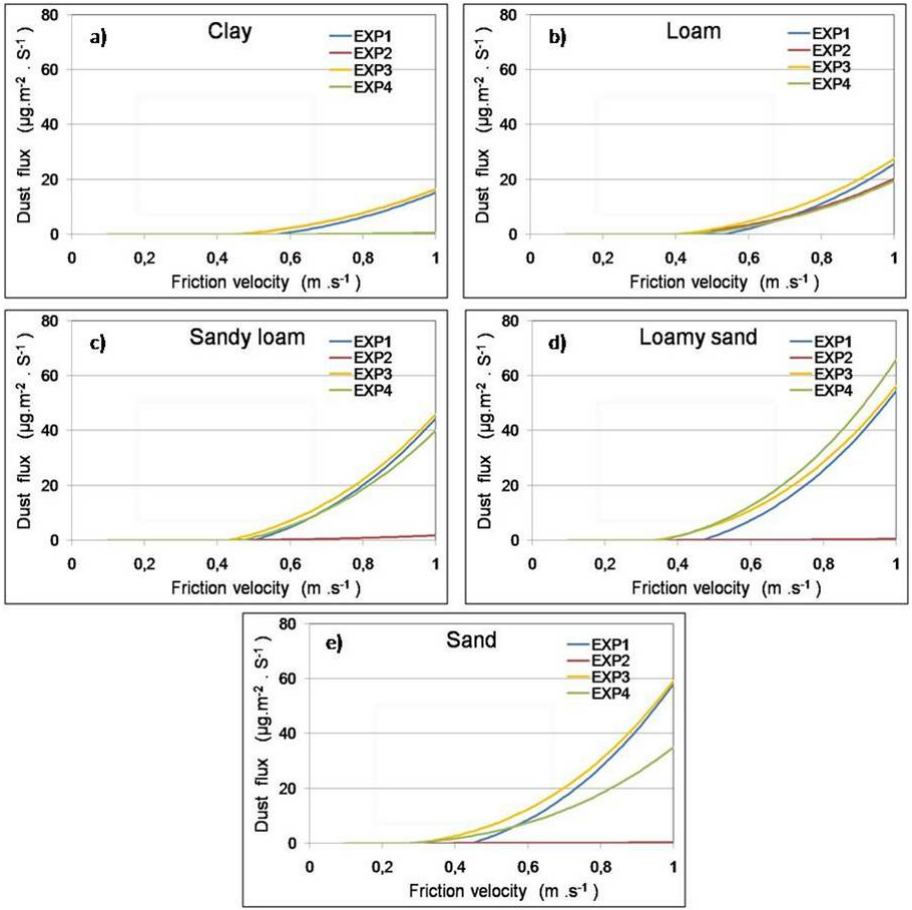

Fig. 6. Evolution of the surface dust fluxes (in $\mu g\, m^{-2}\, s^{-1}$) depending on the friction velocity ($m\, s^{-1}$) over: **(a)** Clay soil **(b)** loam soil, **(c)** sandy loam soil, **(d)** loamy sand soil and **(e)** sand soil.

GMDD
4, 2893–2936, 2011

Importance of the surface size distribution of erodible material

M. Mokhtari et al.

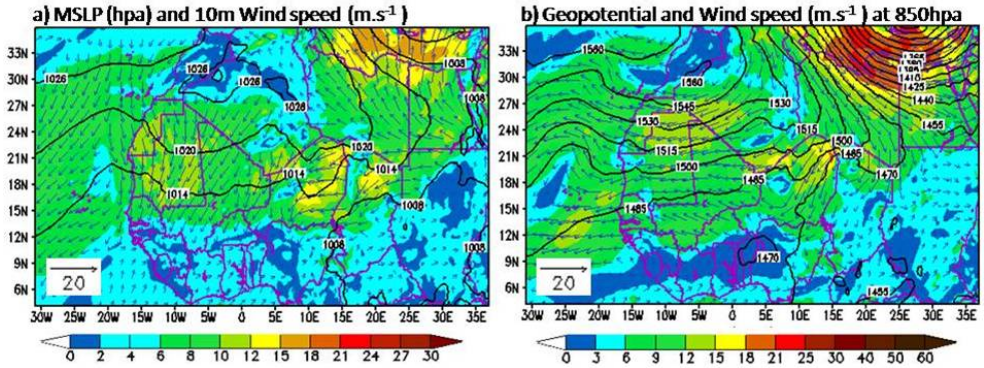

Fig. 7. Mean sea level pressure (hpa) and 10 m wind speed **(a)** and geopotential (in meters) and wind speed at 850 hPa **(b)**, on 8 March 2006 at 12:00 UTC.

GMDD
4, 2893–2936, 2011

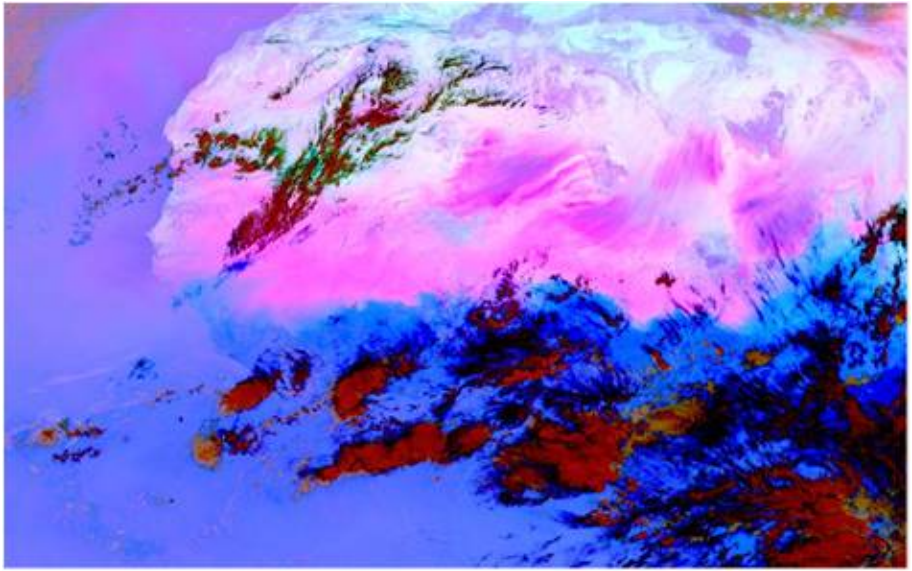

Fig. 8. MSG-SEVIRI satellite image over West Africa for 8 March 2006 at 12:00 UTC, pink color represents for dust, black for cirrus, red for high level cloud, brown for mid-level cloud, and white for desert surface.

GMDD
4, 2893–2936, 2011

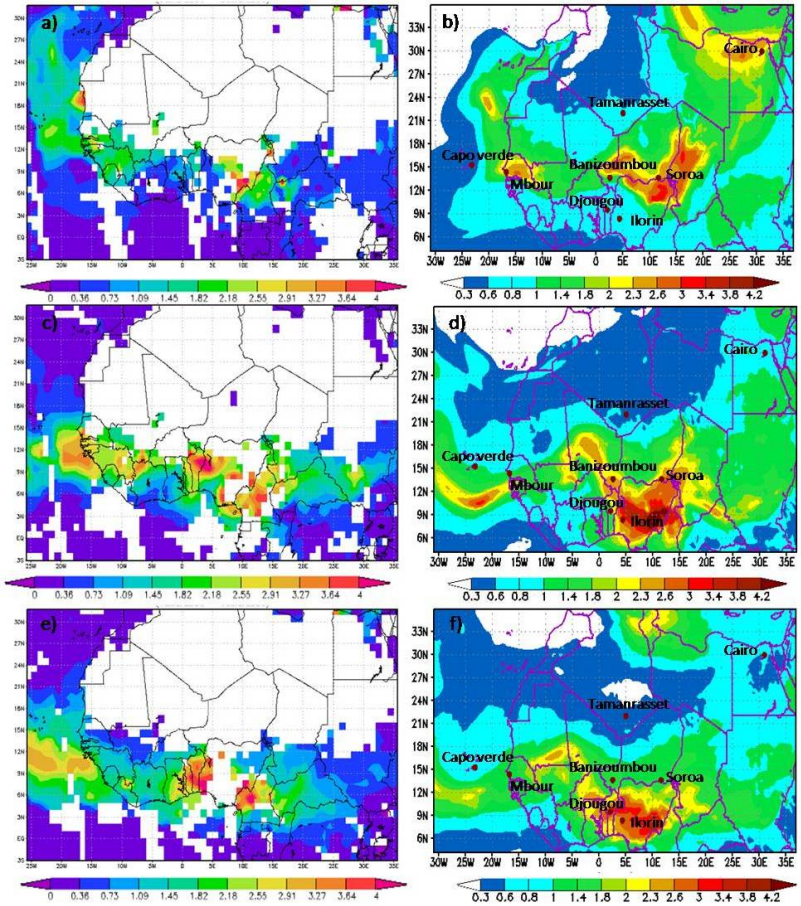

Fig. 9. Daily mean AOD (at 550 nm) from MODIS/AQUA satellite images (**a**, **c** and **e**), respectively, on 8, 10 and 12 March 2006 and daily mean AOD (at 550 nm) simulated by ALADIN (b, d and f) respectively, on 8, 10 and 12 March 2006.

GMDD
4, 2893–2936, 2011

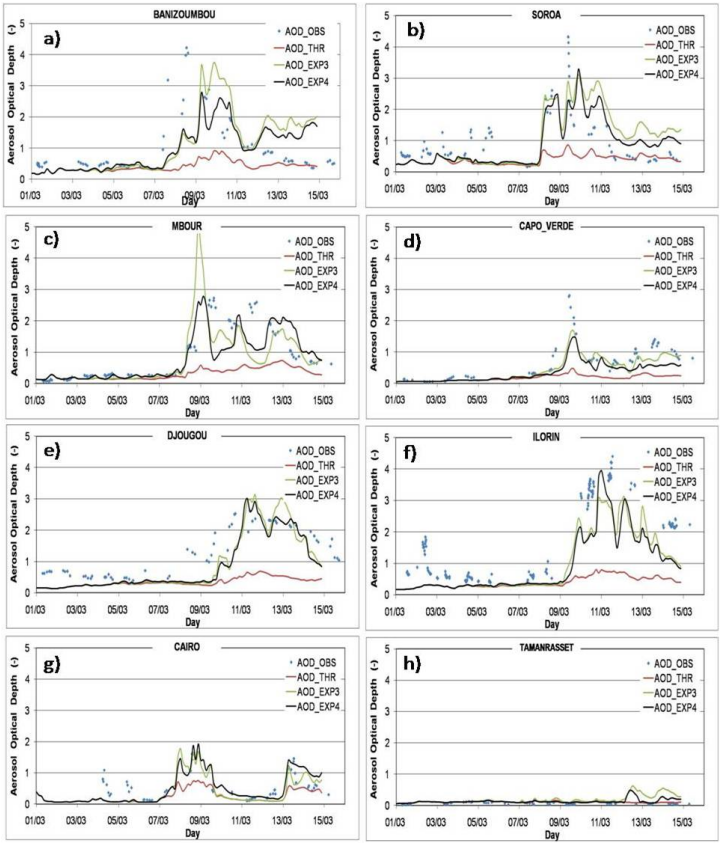

Fig. 10. Evolution of the AOD (at 550 nm) simulated by ALADIN, with three dust emissions schemes: THR (red line), EXP3 (green line) and EXP4 (black line), between 1 and 15 March 2006, over **(a)** Banizoumbou, **(b)** Soroa, **(c)** Mbour, **(d)** Capo Verde, **(e)** Djougou, **(f)** Ilorin, **(g)** Cairo and **(h)** Tamanrasset, compared with AERONET photometer observations AOD_440 (level 2).

GMDD
4, 2893–2936, 2011

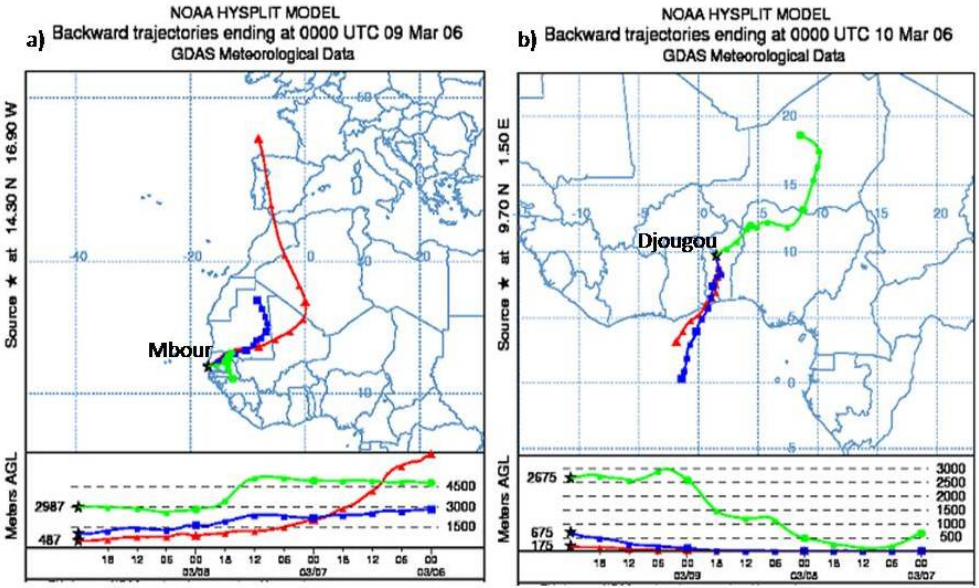

Fig. 11. NOAA Hysplit Model, backward trajectories at the 500 m level (red line), 1000 meter level (blue line) and 3000 m level (green line) ending at: **(a)** 00:00 UTC, 9 March 2006, over Mbour and **(b)** 00:00 UTC, 10 March 2006, over Djougou.

GMDD
4, 2893–2936, 2011

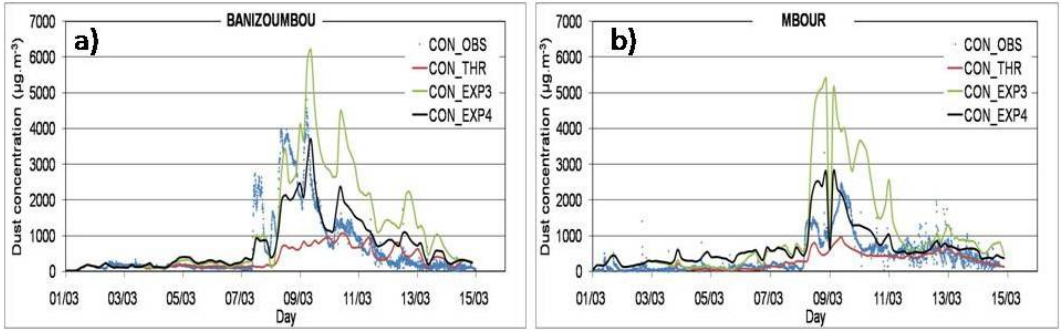

Fig. 12. Evolution of the dust surface concentration in ($\mu g\, m^{-3}$) simulated by ALADIN, with three dust emission configurations: THR (red line), EXP3 (green line) and EXP4 (black line), between 1 and 15 March 2006, over **(a)** Banizoumbou and **(b)** Mbour, compared with the observations.

GMDD
4, 2893–2936, 2011

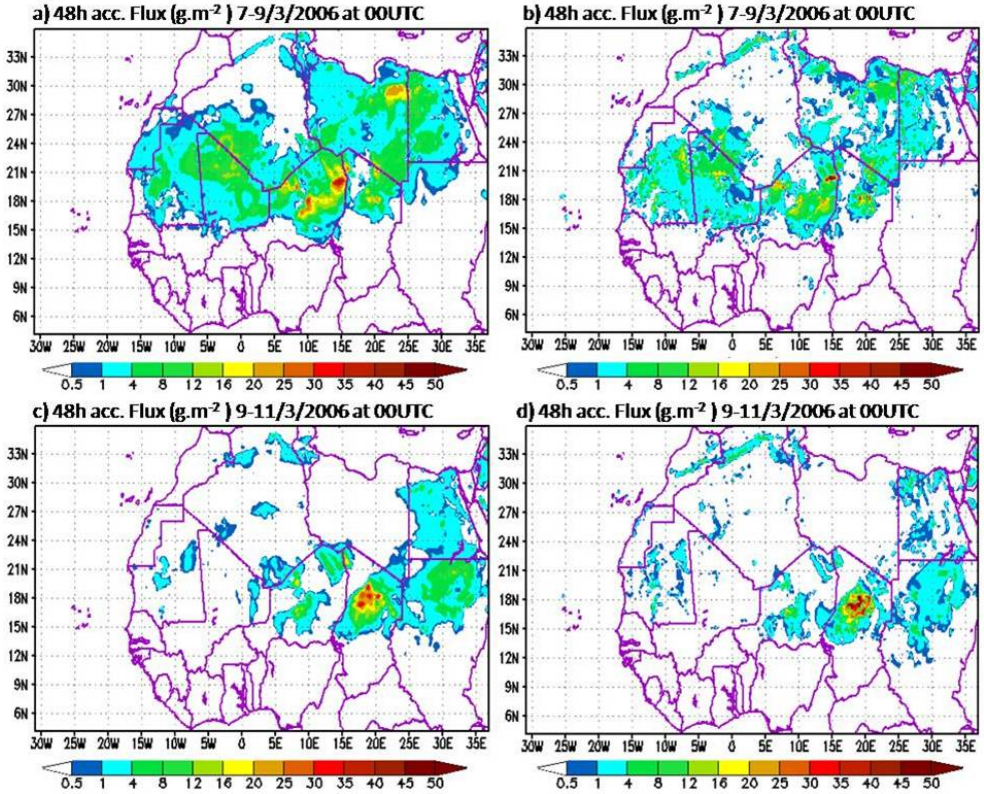

Fig. 13. 48 h accumulated dust fluxes (in g m^{-2}) simulated by ALADIN with EXP3 **(a)** and **(c)** and EXP4 **(b)** and **(d)** for 7–9 March, and 9–11 2006 at 00:00 UTC.

GMDD
4, 2893–2936, 2011